

# JOURNAL OF GLACIOLOGY



**CAMBRIDGE**  
UNIVERSITY PRESS

THIS MANUSCRIPT HAS BEEN SUBMITTED TO THE JOURNAL OF GLACIOLOGY AND HAS NOT BEEN PEER-REVIEWED.

## **A shallow approximation for ice streams sliding over strong beds**

Journal:	<i>Journal of Glaciology</i>
Manuscript ID	Draft
Manuscript Type:	Article
Date Submitted by the Author:	n/a
Complete List of Authors:	Warburton, Kasia; Dartmouth College; University of Cambridge, Department of Applied Mathematics and Theoretical Physics Hewitt, Duncan; University College London, Department of Mathematics Meyer, Colin; Dartmouth College, Thayer School of Engineering Neufeld, Jerome; University of Cambridge, Institute of Theoretical Geophysics, Department of Applied Mathematics and Theoretical Physics; University of Cambridge, BP Institute; University of Cambridge, Department of Earth Sciences, Bullard Laboratories
Keywords:	Glacial rheology, Glacier flow, Ice dynamics, Ice streams
Abstract:	Ice streams are regions of rapid ice sheet flow characterised by a high degree of sliding over a deforming bed. The Shallow Shelf Approximation (SSA) provides a convenient way to obtain closed-form approximations of the velocity and flux in a rapidly-sliding ice stream when the basal drag is much less than the driving stress. However, the validity of the SSA approximation breaks down when the magnitude of the basal drag increases. Here we find a more accurate expression for the velocity and

	flux in this transitional regime before vertical deformation fully dominates, in agreement with numerical results. The closed-form expressions we derive can be incorporated into wider modelling efforts to yield a better characterisation of ice stream dynamics, and inform the use of the SSA in large-scale simulations.

SCHOLARONE™  
Manuscripts

# A shallow approximation for ice streams sliding over strong beds

Katarzyna L.P. WARBURTON<sup>1</sup>, Duncan R. HEWITT<sup>2</sup>, Colin R. MEYER<sup>1</sup>, Jerome A.  
NEUFELD<sup>3,4</sup>

<sup>1</sup>*Thayer School of Engineering, Dartmouth College, NH, USA*

<sup>2</sup>*Department of Mathematics, University College London, London, UK*

<sup>3</sup>*Department of Earth Sciences, University of Cambridge, Cambridge, UK*

<sup>4</sup>*Department of Applied Mathematics and Theoretical Physics, University of Cambridge, Cambridge, UK*

*Correspondence: Kasia Warburton <kasia.warburton@dartmouth.edu>*

**ABSTRACT.** Ice streams are regions of rapid ice sheet flow characterised by a high degree of sliding over a deforming bed. The Shallow Shelf Approximation (SSA) provides a convenient way to obtain closed-form approximations of the velocity and flux in a rapidly-sliding ice stream when the basal drag is much less than the driving stress. However, the validity of the SSA approximation breaks down when the magnitude of the basal drag increases. Here we find a more accurate expression for the velocity and flux in this transitional regime before vertical deformation fully dominates, in agreement with numerical results. The closed-form expressions we derive can be incorporated into wider modelling efforts to yield a better characterisation of ice stream dynamics, and inform the use of the SSA in large-scale simulations.

## INTRODUCTION

Numerical simulations of the flow of shear-thinning ice over the complex topography of ice sheet beds using 3-dimensional full-Stokes models are computationally expensive, while in a wide variety of scenarios the geometry of the situation suggests natural simplifications. Ice is often much shallower than the horizontal scales on which basal conditions and driving stresses vary, motivating shallow approximations

26 where pressure gradients are hydrostatic (Cuffey and Paterson, 2010; Fowler, 2011). If the ice is frozen to  
27 the bed and vertical shear dominates the deformation, the Shallow Ice Approximation (SIA) accurately  
28 captures the dynamics. In fast-flowing regions of ice sheets where basal resistance is low, the dominant  
29 stresses are a combination of extensional stress and lateral shear, so the Shallow Shelf Approximation (SSA)  
30 or depth-integrated membrane models provide lower-dimensional formulations (Morland, 1987; MacAyeal,  
31 1989; Blatter, 1995; Pattyn, 2003; Hindmarsh, 2004).

32 In simple geometries, such as wide, uniform ice streams, a further advantage of the SIA and SSA models  
33 is that they can be solved exactly to give closed-form expressions for the ice velocity and flux (Raymond,  
34 1996). These expressions can then be used as a simple, essentially 1D representation of ice dynamics in models  
35 of related dynamical processes, such as the response of tidewater glaciers to calving (Benn and others, 2007),  
36 the impact of basal melt during Heinrich events (Mann and others, 2021), or interactions of the ice with  
37 its bed at the start of surges (Minchew and Meyer, 2020). However, the simplified expressions for the  
38 velocity and flux of ice have often been used beyond the regimes in which they are asymptotically valid, in  
39 particular in the transition from SSA to SIA as basal drag increases. Simply summing the two expressions  
40 (e.g. Mann and others, 2021) as an ad-hoc transition does not correctly capture the particular dynamics  
41 occurring in this rapidly-sliding, high basal shear regime, as we show numerically and mathematically in  
42 this work. Furthermore, by understanding the transition between these flow regimes, the detailed flow  
43 profiles may be used to infer basal properties.

44 Small amounts of basal drag, such as would be experienced by an ice stream sliding over a bed of  
45 yielding sediment, can be viewed as a perturbation to the SSA expression for freely-sliding flow. A natural  
46 question is at what point the flow becomes significantly modified, and whether this happens before reaching  
47 the fully non-sliding regime. Schoof and Hindmarsh (2010) mathematically examined the effect of basal  
48 drag as a higher-order correction to purely extensional flow. Here, motivated by the geometry of ice streams  
49 and their importance in wider models of climate dynamics, we look instead at the case where the dominant  
50 resistance to flow comes from lateral shear at the sidewalls, and the rheology of the shear margins are the  
51 primary control on the velocity of the stream (Meyer and Minchew, 2018; Hunter and others, 2021).

52 Since ice is shear-thinning, basal drag impacts not just the overall force balance but also the depth-  
53 averaged rheology. This motivates the "L1L2" modelling framework (Hindmarsh, 2004) in which a linear  
54 approximation to the vertical shear acts to modify the ice viscosity. This framework has been implemented  
55 in large-scale ice sheet models to capture ice flow dynamics lying between the SSA and SIA regimes (Gold-

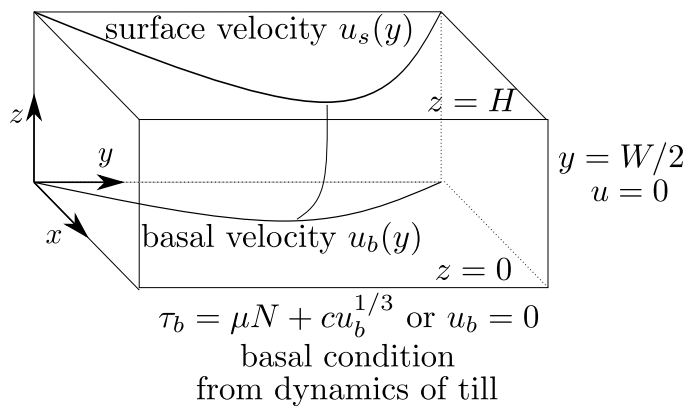


**Fig. 1.** Diagram of the ice stream geometry

56 berg and Sergienko, 2011). The hybrid model captures the transition between SSA and SIA in a less  
 57 computationally intensive way than full-Stokes simulations, but remains a predominantly numerical tech-  
 58 nique. Here we mathematically analyse the "L1L2" method to derive simple, yet more accurate expressions  
 59 for the ice velocity and flux in this transitional regime.

60 In this paper we look at the flow of shear-thinning ice over a bed of uniform shear strength, through  
 61 a wide, shallow rectangular stream. We use asymptotic analysis to derive closed-form expressions for the  
 62 velocity field and flux through the stream, both when basal resistance is small and as it increases towards  
 63 the driving stress. We show that these expressions recover both the SSA and SIA limits as expected, but  
 64 we also obtain a new, intermediate regime in which basal shear-softening is significant. We further solve  
 65 for the flow-field numerically, confirming the existence of this regime, and show that our new expression  
 66 significantly reduces the error in predicted velocities.

## 67 GOVERNING EQUATIONS AND APPROACH

68 We consider the steady flow of shear-thinning ice in a shallow, rectangular channel which is uniform in the  
 69 along-flow direction (figure 1). This means the pressure is hydrostatic, and the velocity field is only in the  
 70 along-stream direction,  $\mathbf{u} = (u(y, z), 0, 0)$ . As the flow is uniform in this direction, we have no extensional  
 71 strains in this geometry, a simplification that allows us to retain and evaluate the impact of vertical strain  
 72 instead. While longitudinal and vertical strains can become comparable if basal resistance is very low  
 73 and the along-stream variation is large, along-stream changes in velocity often occur over length scales  
 74 much greater than the width or depth of ice streams, with extensional stresses effectively acting to smooth  
 75 variations in driving stress (Kamb and Echelmeyer, 1986).

Given these assumptions, the stress field within the ice satisfies

$$\frac{\partial \tau_{xy}}{\partial y} + \frac{\partial \tau_{xz}}{\partial z} = -\frac{\tau_d}{H}, \quad (1)$$

where the driving stress,

$$\tau_d = \rho_i g H \frac{\partial S}{\partial x}, \quad (2)$$

is due to gradients in surface height  $S$ . We take a power-law shear-thinning rheology for the ice

$$e_{ij} = A \tau^{n-1} \tau_{ij}, \quad e_{ij} = \frac{1}{2} (\nabla \mathbf{u} + \nabla \mathbf{u}^T), \quad \tau = \sqrt{\frac{1}{2} \tau_{ij} \tau_{ij}}, \quad (3)$$

76 where  $A$  is the viscosity prefactor, which in general may be a function of temperature and grain size, but  
 77 here we take as constant. The shear-thinning exponent  $n$  is usually taken to be 3 for ice (Glen, 1955),  
 78 although using values from 1.8 to 4 represents the different modes of deformation that make up ice flow  
 79 (Goldsby and Kohlstedt, 2001; Millstein and others, 2022). Even higher effective shear exponents could  
 80 represent the effect of damage or shear heating in the margins of the ice stream, where high shear rates  
 81 warm and soften the ice further (Minchew and others, 2017). We will show numerical results for  $n = 3$ ,  
 82 but give expressions for general  $n$  as far as possible.

### 83 Boundary conditions

84 On the two sidewalls  $y = \pm W/2$  we apply a no-slip boundary condition, motivated by fact that ice streams  
 85 and glaciers are usually either topographically constrained between high bedrock or surrounded by much  
 86 slower-flowing ice. At the upper surface of the ice,  $z = H$ , we impose a no-stress condition as the ice is  
 87 in contact with the atmosphere. At the base of the stream  $z = 0$ , we link the basal shear stress,  $\tau = \tau_b$ ,  
 88 to the basal sliding speed,  $u = u_b$ , through a sliding law representing the rheology and/or geometry of the  
 89 bed in contact with the base of the ice stream.

Over beds of deformable sediment, an appropriate basal boundary condition is a plastic traction law,

$$\tau_b = \mu N, \quad u_b > 0, \quad (4)$$

$$\tau_b < \mu N, \quad u_b = 0, \quad (5)$$

90 where  $\mu$  is a friction coefficient and  $N = p_i - p_w$  is the effective pressure, which is the difference between

91 the pressure exerted by the weight of the ice  $p_i$  and the water pressure in the pore space  $p_w$ . This will  
 92 form the basis for our analysis here, since deformable sediments are found below many fast-flowing streams  
 93 (Kamb, 2001; Iverson, 2010).

However, in large-scale models, the basal shear stress and sliding speed are often related via a power-law,

$$\tau_b = C u_b^{1/m}, \quad (6)$$

94 originally derived from ice sliding over a hard bed with small-scale topography (Weertman, 1957) but now  
 95 extended to other scenarios by modifying the value of the exponent  $m$ . Large values of  $m \geq 8$  have been  
 96 used to approximate plastic deformation (Rosier and others, 2015; Minchew and others, 2016; Joughin and  
 97 others, 2019). A numerical study of the impact of this power-law sliding in a similar channel geometry is  
 98 given in Adhikari and Marshall (2012), and we will discuss the value of our plastic bed calculations for  
 99 reproducing these results.

100 If the basal shear stress  $\tau_b$  is large compared to the driving stress  $\tau_d$ , equation (5) reduces to a bed that  
 101 is unyielded everywhere, and we obtain a no-slip boundary condition,  $u_b = 0$ , as would be the case in the  
 102 SIA. When  $\tau_b \rightarrow 0$ , we recover a no-stress basal boundary condition, where the SSA is strictly valid. In  
 103 this paper we recover both of these well-known limits but focus on the intermediate regime where  $u_b$  and  
 104  $\tau_b/\tau_d$  are both large. We seek to find closed-form approximations for the ice velocity field, in particular the  
 105 surface speed  $u_s$ , basal sliding  $u_b$ , and total ice flux  $Q$ , as a function of the width  $W$  and height  $H$  of the  
 106 stream, the shear thinning exponent  $n$ , and the ratio of basal shear stress to driving stress  $\tau_b/\tau_d$ .

Our benchmark will be the expressions for centreline surface velocity and flux obtained by simply  
 summing the SIA and SSA results,

$$u_{mid}^0 = \frac{2AH}{n+1} \left[ (\tau_d - \mu N)^n \frac{W/2^{n+1}}{H} + \mu N^n \right], \quad (7)$$

$$Q^0 = \frac{4AH^2}{n+2} \left[ (\tau_d - \mu N)^n \frac{W/2^{n+2}}{H} + \mu N^n \frac{W/2}{H} \right], \quad (8)$$

107 which neglect the effect of basal shear softening. Our goal is to improve on the accuracy of these results  
 108 while still retaining a closed-form expression.

109 **NUMERICAL METHOD**

We numerically solve for the flow of ice in a rectangular channel with variable basal traction to assess the accuracy of our asymptotic expressions. We use COMSOL to solve (1) in the half-channel  $0 < y < W/2$ ,  $0 < z < H$ , invoking the symmetry of the flow, as a generalised Poisson equation for  $u$ . The effective viscosity is regularised by the addition of a small constant  $\epsilon_1 = 10^{-9}$  to prevent divergence at  $z = H$ ,  $y = 0$ ,

$$\nabla \cdot \left( \frac{1}{2A} (\tau_{xz}^2 + \tau_{xy}^2 + \epsilon_1)^{(1-n)/2} \nabla u \right) = -\frac{\tau_d}{H}. \quad (9)$$

The boundary conditions are no-stress on  $y = 0$  and  $z = H$ , no-slip on  $y = W/2$ , and a traction law on  $z = 0$  that represents a regularised form of (5),

$$\tau_{xz} = \mu N \tanh \left( \frac{u}{\epsilon_2} \right). \quad (10)$$

110 We used an automatically generated triangular mesh on COMSOL's extra-fine setting (5 grid points  
111 across the depth of the stream), and with relative error for convergence of  $10^{-5}$ . The regularisation  
112 parameters  $\epsilon_1 = 10^{-9}$  and  $\epsilon_2 = 10^{-4}$  were also chosen such that decreasing their value by an order of  
113 magnitude did not affect the calculated velocities by more than a factor of  $10^{-5}$ .

114 The numerical results are not the focus of this work but serve as a benchmark for our derived expressions  
115 for velocity and flux, as described in the following sections.

116 **MATHEMATICAL METHOD**

To begin our mathematical analysis of (1), we start by depth-integrating the equation to get

$$\frac{\partial}{\partial y} \int_0^z \tau_{xy} dz + \tau_{xz} - \tau_b = -\tau_d \frac{z}{H}, \quad (11)$$

where  $\tau_b$  is the basal traction, which here is the integration constant found by evaluating this expression at  $z = 0$ . Evaluating (11) at  $z = H$ , where  $\tau_{xz} = 0$ , we find that

$$\frac{\partial}{\partial y} \int_0^H \tau_{xy} dz - \tau_b = -\tau_d. \quad (12)$$



Where the bed is yielded, so that  $\tau_b = \mu N$  uniformly, we can integrate across the stream to arrive at

$$-(\tau_d - \mu N)y = \int_0^H \tau_{xy} dz, \quad (13)$$

and so the problem reduces to evaluating the depth-integrated lateral shear stress, and in particular evaluating the relative effects of vertical and lateral shear on the viscosity.

### Approximation of vertical shear stress and viscosity

If basal sliding is significant across the width of the channel, we assume that gradients in the surface velocity profile  $u_s(y)$  provide an accurate reflection of the lateral shear rate throughout the full depth of the ice.

Motivated by numerically calculated stress fields (figure 2), the much larger horizontal than vertical lengthscales, and the approach of Hindmarsh (2004), we further assume that the vertical shear stress that feeds into the rheology is approximately linear with depth. Hence we may approximate the lateral and vertical shear stresses, and hence the ice rheology, as

$$\tau_{xy} = \tilde{\eta} \frac{\partial u_s}{\partial y}, \quad \tilde{\tau}_{xz} = \mu N \frac{H - z}{H}, \quad (14)$$

$$\tilde{\eta} = \frac{1}{2A} (\tilde{\tau}_{xz}^2 + \tau_{xy}^2)^{(1-n)/2}, \quad (15)$$

where the tilde denotes that this is now based on the approximate vertical shear stress. This is similar to the L1L2 model of Hindmarsh (2004) but here vertical shear stresses are scaled with  $\mu N$  rather than  $\tau_d$ .

### Horizontal shear rate

Writing  $\tilde{\eta} = \tau_{xy} / \frac{\partial u_s}{\partial y}$ , we can approximate equations (14-15) in two limits depending on the relative sizes of  $\tau_{xy}$  and  $\tilde{\tau}_{xz}$ . If vertical shear stresses are much greater than horizontal,  $\tilde{\tau}_{xz} \gg \tau_{xy}$ ,

$$\tau_{xy} \approx \left( \mu N \frac{H - z}{H} \right)^{1-n} \frac{1}{2A} \frac{\partial u_s}{\partial y}, \quad (16)$$

which exhibits strong depth-dependence. In contrast, if lateral shear stresses are much greater than vertical,

$$\tau_{xy} \gg \tilde{\tau}_{xz},$$

$$\tau_{xy} \approx \left( \frac{1}{2A} \frac{\partial u_s}{\partial y} \right)^{1/n}, \quad (17)$$

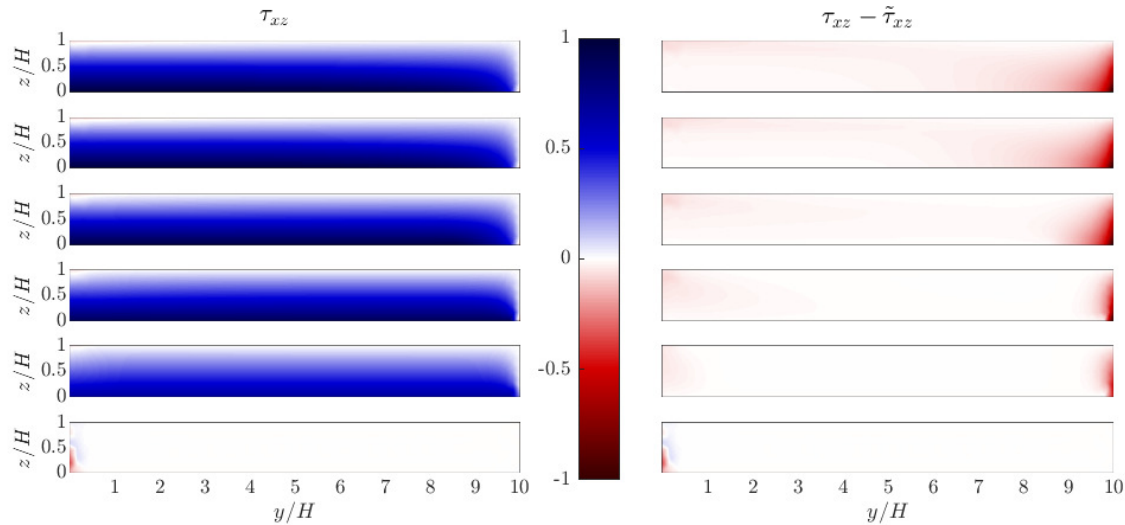


**Fig. 2.** Left, numerically calculated  $\tau_{xz}$ , and right, difference between  $\tau_{xz}$  and the approximation  $\tilde{\tau}_{xz}$  (14), for increasing values of  $1 - \mu N/\tau_d = 10^{-2.5}, 10^{-2}, 10^{-1.5}, 10^{-1}, 10^{-0.5}, 1$ . All values are scaled so that  $\tau_d = 1$ . The agreement is generally excellent, but  $\tau_{xz}$  is noticeably less than  $\tilde{\tau}_{xz}$  in a region  $O(H)$  near the sidewall, and over unyielded regions of the bed where  $\tau_b < \mu N$ . Near the centre of the stream the divergence of viscosity leads to error in the numerically calculated field (particularly visible when  $\mu N = 0$  and the exact solution is  $\tau_{xz} = 0$  everywhere). All for  $W/2H = 10$  and  $n = 3$ .

126 which is uniform in depth.

We define a transition depth  $z_t$  at which a transition in the dominant stress occurs, and below which basal shear dominates, given by

$$\left(\mu N \frac{H - z_t}{H}\right) \sim \left(\frac{1}{2A} \frac{\partial u_s}{\partial y}\right)^{1/n}. \quad (18)$$

Thus the leading order expression for the depth-integrated stress is given by integrating the dominant term in each region,

$$-(\tau_d - \mu N)y = \int_0^H \tau_{xy} dz \quad (19)$$

$$= \int_{z_t}^H \left(\frac{1}{2A} \frac{\partial u_s}{\partial y}\right)^{1/n} dz + \int_0^{z_t} \left(\mu N \frac{H - z}{H}\right)^{1-n} \frac{1}{2A} \frac{\partial u_s}{\partial y} dz \quad (20)$$

$$= (H - z_t) \left(\frac{1}{2A} \frac{\partial u_s}{\partial y}\right)^{1/n} + \frac{H}{(n-2)\mu N} \left(\mu N \frac{H - z_t}{H}\right)^{2-n} \frac{1}{2A} \frac{\partial u_s}{\partial y} - \frac{H(\mu N)^{1-n}}{n-2} \frac{1}{2A} \frac{\partial u_s}{\partial y} \quad (21)$$

$$\sim \frac{n-1}{n-2} \frac{H}{\mu N} \left(\frac{1}{2A} \frac{\partial u_s}{\partial y}\right)^{2/n} \quad \text{if } \frac{\partial u_s}{\partial y} \ll 2A(\mu N)^n, \quad (22)$$

or if  $z_t \leq 0$  then lateral shear dominates the viscosity everywhere, so

$$-(\tau_d - \mu N)y = \int_0^H \tau_{xy} dz = \int_0^H \left( \frac{1}{2A} \frac{\partial u_s}{\partial y} \right)^{1/n} dz \quad (23)$$

$$= H \left( \frac{1}{2A} \frac{\partial u_s}{\partial y} \right)^{1/n} \quad \text{if } \frac{\partial u_s}{\partial y} > 2A(\mu N)^n. \quad (24)$$

If  $\mu N \ll \tau_d$ , then (24) applies almost everywhere and the leading order expression for the surface velocity profile is given by

$$u_s \approx \frac{2A}{(n+1)} \frac{(\tau_d - \mu N)^n}{H^n} [(W/2)^{n+1} - y^{n+1}], \quad (25)$$

127 which is the SSA approximation for an ice stream with constant basal traction  $\mu N$  (Raymond, 1996).  
 128 While the modification to  $\tau_d$  is negligible in the limit for which (25) is asymptotically valid, this expression  
 129 is used even when  $\mu N \sim \tau_d$  (e.g. Minchew and others, 2018).

130 However, as basal drag increases, the vertical shear stress starts to dominate in the central region of  
 131 the stream where lateral stresses are lowest. This shear-softening decreases the depth-integrated viscosity,  
 132 and leads to a significant increase in velocity compared to the prediction of the SSA approach (figure 3).

133 The SSA result becomes an even poorer approximation as basal drag increases further, and the bed  
 134 becomes unyielded over a significant portion of the stream. Using (13), which assumes that  $\tau_b = \mu N$   
 135 everywhere, overestimates the resistance to flow and thus additionally underestimate the ice velocity; to  
 136 correct this we must look further at the vertical structure of the flow.

### 137 Vertical shear rate and basal boundary condition

138 Now that we have a measure of both  $\tau_{xy}$  and  $\tau_{xz}$ , we can calculate the effective viscosity and thus evaluate  
 139 the vertical deformation of the ice by finding  $\partial u / \partial z$ . This allows us to estimate the basal velocity  $u_b$  and  
 140 to better characterise whether the bed should be yielded ( $\tau_b = \mu N$ ) or unyielded ( $u_b = 0$ ).

At the sides of the stream, where lateral shear dominates the viscosity, and still approximating the vertical shear stress as linear in depth, we have that

$$\tau_{xz} = \mu N \frac{H-z}{H} = \eta \frac{\partial u}{\partial z} = \frac{1}{2A} \left[ (\tau_d - \mu N) \frac{y}{H} \right]^{1-n} \frac{\partial u}{\partial z}, \quad (26)$$

$$u = u_s(y) - \frac{2A}{2} \mu N \frac{(H-z)^2}{H} \left[ (\tau_d - \mu N) \frac{y}{H} \right]^{n-1}, \quad (27)$$

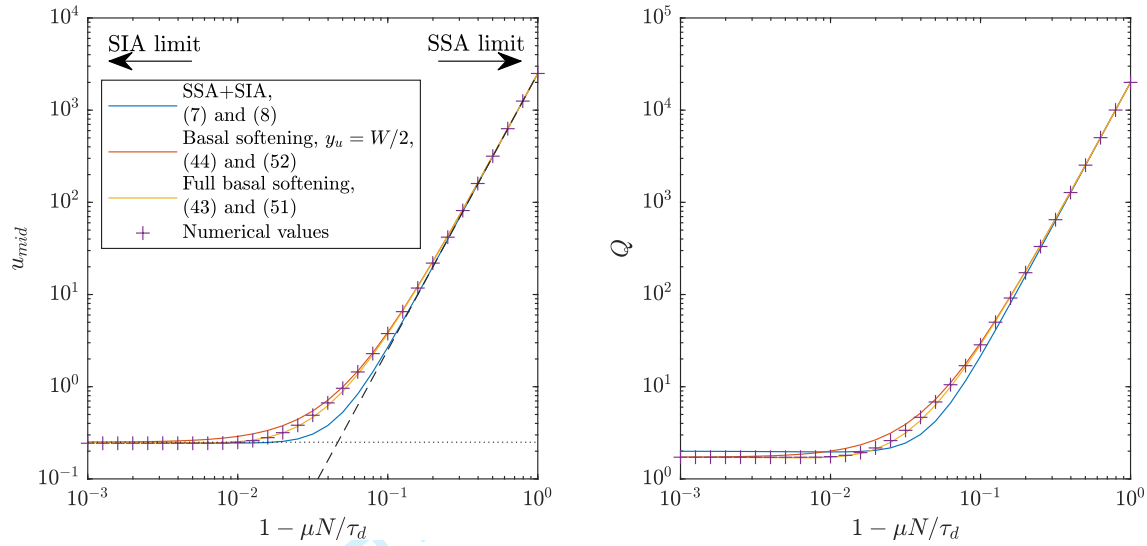


**Fig. 3.** Including shear softening improves the match to numerically calculated values of a) the centreline surface velocity  $u_s(0)$  and b) the total flux  $Q$ , particularly when  $\tau_d - \mu N \sim 0.1\tau_d$ . Here  $W/2 = 10H$  and  $n = 3$ . SSA and SIA limits of the surface velocity are shown as dashed and dotted lines.

so that the basal sliding speed is

$$u_b(y) = \frac{2AH(\tau_d - \mu N)^n}{(n+1)} \left[ \left( \frac{W/2}{H} \right)^{n+1} - \left( \frac{y}{H} \right)^{n+1} - \frac{(n+1)\mu N}{2(\tau_d - \mu N)} \left( \frac{y}{H} \right)^{n-1} \right]. \quad (28)$$

Note that this becomes negative very close to  $y = W/2$ ; in effect this determines the point beyond which the bed is unyielded and  $u_b = 0$  should apply instead of  $\tau_b = \mu N$ . We can find the approximate edge of the unyielded region  $y = y_u$  by solving  $u_b(y_u) = 0$ , so that

$$\left( \frac{W}{2} \right)^{n+1} = y_u^{n+1} + \frac{(n+1)\mu NH^2}{2(\tau_d - \mu N)} y_u^{n-1}. \quad (29)$$

To leading order in  $W/2 - y_u$  we can solve for  $y_u$  approximately and get

$$y_u = \frac{W}{2} - \frac{\mu NH^2}{2(\tau_d - \mu N)(W/2)}, \quad (30)$$

141 which, for its simplicity, we will use through the rest of the paper. Figure 4 shows that (30) accurately  
 142 captures the behaviour as  $y_u \rightarrow W/2$ , as well as agreeing that  $y_u \rightarrow 0$  as  $\mu N \rightarrow \tau_d$ , but determining the  
 143 exact boundary of the yielded bed is a free boundary problem (Schoof, 2006) and in general can only be  
 144 solved for numerically.

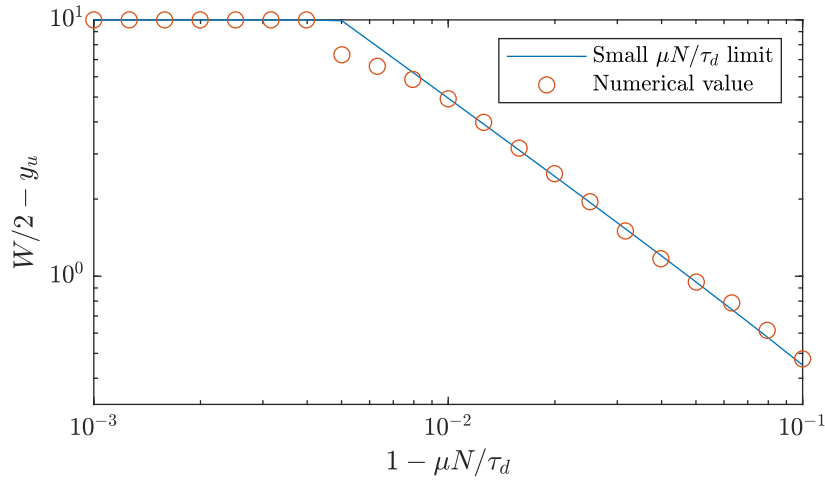


**Fig. 4.** Match between the approximate expression for  $y_u$  (30), and the numerically calculated edge of the yielded bed, for  $W/2 = 10H$ ,  $n = 3$ . The disagreement at larger  $\mu N$  is expected since when  $y_u$  moves away from the sidewalls the approximations that lead to (29) no longer hold, but (30) does capture that  $y_u \rightarrow 0$  there.

To find the internal deformation in the centre of the stream, where basal shear starts to play a role, there are two regimes to consider: below  $z_t$  the basal shear dominates, while close to the surface the lateral shear sets the viscosity. Considering only these dominant contributions to the viscosity, we can obtain the leading order approximation to  $\partial u/\partial z$  above  $z_t$  by

$$\tau_{xz} = \mu N \frac{H-z}{H} = \eta \frac{\partial u}{\partial z} = \frac{1}{2A} \left[ \frac{n-2}{n-1} \mu N (\tau_d - \mu N) \frac{y}{H} \right]^{\frac{1-n}{2}} \frac{\partial u}{\partial z}, \quad (31)$$

$$u = u_s(y) - \frac{2A}{2} \mu N \frac{(H-z)^2}{H} \left[ \frac{n-2}{n-1} \mu N (\tau_d - \mu N) \frac{y}{H} \right]^{\frac{n-1}{2}}, \quad (32)$$

$$u(z_t) = u_s(y) - \frac{2A}{2} \frac{H}{\mu N} \left[ \frac{n-2}{n-1} \mu N (\tau_d - \mu N) \frac{y}{H} \right]^{\frac{n+1}{2}}, \quad (33)$$

while below  $z_t$  we have

$$\tau_{xz} = \mu N \frac{H-z}{H} = \eta \frac{\partial u}{\partial z} = \frac{1}{2A} \tau_{xz}^{1-n} \frac{\partial u}{\partial z}, \quad (34)$$

$$u = u(z_t) - \frac{2A}{n+1} \mu N^n H \left[ \left( \frac{H-z}{H} \right)^{n+1} - \left( \frac{n-2}{n-1} \frac{\tau_d - \mu N}{\mu N} \frac{y}{H} \right)^{\frac{n+1}{2}} \right]. \quad (35)$$

Thus the basal velocity is

$$u_b = u_s(y) - \frac{2A}{n+1} H \mu N^n \left[ 1 + \frac{n-1}{2} \left( \frac{n-2}{n-1} \frac{\tau_d - \mu N}{\mu N} \frac{y}{H} \right)^{\frac{n+1}{2}} \right]. \quad (36)$$

Note that the deformation velocity,  $u_d = u_s - u_b$  is

$$u_d = \frac{2A}{n+1} H \mu N^n \left[ 1 + \frac{n-1}{2} \left( \frac{n-2}{n-1} \frac{\tau_d - \mu N}{\mu N} \frac{y}{H} \right)^{\frac{n+1}{2}} \right]. \quad (37)$$

145 The first term is the SIA surface speed, and is larger than the second term until the very edges of this  
146 central, basal drag dominated region.

## 147 RESULTS

### 148 Surface velocity and sliding speed

We now combine our expressions for stress and velocity to obtain the surface velocity at the centreline of the ice stream. We have calculated the horizontal shear rate over the yielded regions where  $\tau_b = \mu N$ , the extent  $y_u$  of the unyielded region of the bed, and the vertical shear at the edge of this region, where both  $u_b = 0$  and  $\tau_b = \mu N$ . Thus, we integrate up from the bed at  $y_u$  to find  $u_s(y_u)$ , then integrate inwards to find the surface velocity profile over the yielding region, giving

$$u_{mid} = \int_0^H \frac{\partial u}{\partial z} \Big|_{y=y_u} dz + \int_0^{y_u} \frac{\partial u_s}{\partial y} dy. \quad (38)$$

There are two regimes to consider depending on the dominant contribution to the depth-integrated viscosity at  $y_u$ . When the basal drag is small, (24) dominates and we have a small modification to the SSA solution,

$$u_s \approx 2AH \frac{(\tau_d - \mu N)^n}{n+1} \left[ \left( \frac{y_u}{H} \right)^{n+1} - \left( \frac{y}{H} \right)^{n+1} + \frac{\mu N}{2(\tau_d - \mu N)} \left( \frac{y_u}{H} \right)^{n-1} \right], \quad (39)$$

Since  $y_u$  is very close to  $W/2$ , and  $\tau_d - \mu N \gg \mu N$ , the deformation velocity is small compared to the horizontal shear and so that the leading order expression for the centreline velocity is exactly the SSA result of

$$u_{mid} \approx 2AH \frac{(\tau_d - \mu N)^n}{n+1} \left( \frac{W/2}{H} \right)^{n+1}, \quad (40)$$

149 and this is also the leading order term in  $u_b$ .

When the basal drag is large, (22) dominates the horizontal shear, and so

$$u_{mid} \approx 2AH \left[ \frac{2}{n+2} \left( \frac{n-2}{n-1} \mu N (\tau_d - \mu N) \right)^{n/2} \left( \frac{y_u}{H} \right)^{(n+2)/2} + \frac{\mu N^n}{n+1} \right] \quad (41)$$

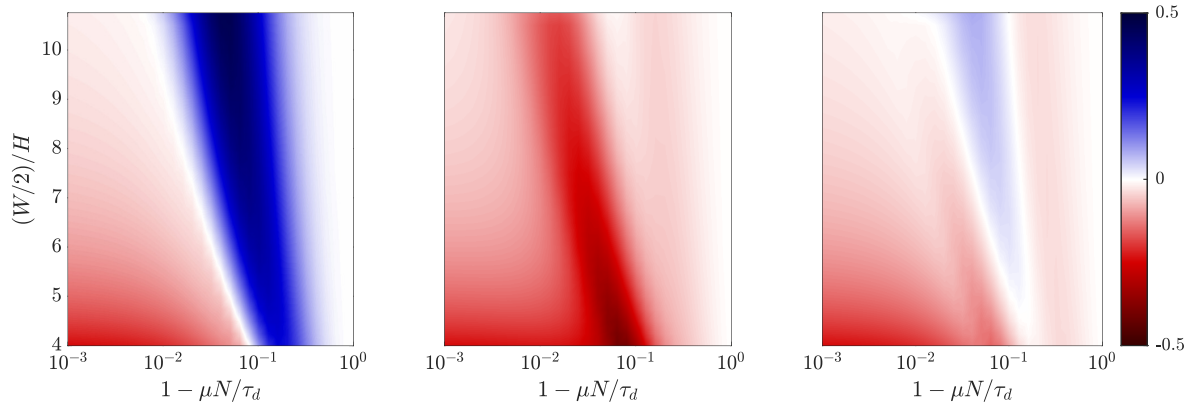


**Fig. 5.** Fractional error in expressions for  $u_{mid}$  as compared to the numerically calculated values (1 - expression/numerical value, so overestimates are negative errors), for a range of aspect ratios and basal strengths, with  $n = 3$ . a) Sum of SIA and SSA, equation (7), b) including basal shear softening, but with  $y_u$  set to  $W/2$  (44), and c) the full expression (43). Both b) and c) represent improvements over a), with c) the closest match to the numerical results. When the aspect ratio is not large, all the approximations start to break down. The maximum error in b) is  $-0.40$  at  $W/2H = 4$  but reduces to  $-0.17$  at  $W/2H = 11$ . The error in c) ranges from  $-0.24$  to  $0.085$  but remains within  $\pm 0.1$  for  $W/2H > 5.75$ .

while

$$u_b(0) \approx \frac{4AH}{n+2} \left( \frac{n-2}{n-1} \mu N (\tau_d - \mu N) \right)^{n/2} \left( \frac{y_u}{H} \right)^{(n+2)/2}. \quad (42)$$

150 Using the expression for  $y_u$  from (30), we find that (41) provides a good match to the numerical results  
 151 when  $\tau_d - \mu N \ll \tau_d$  (figure 5).

We suggest that an appropriate expression for the centreline velocity that transitions smoothly between the two regimes can be found by adding together (40) and (41), giving

$$u_{mid} \approx 2AH \left[ \frac{(\tau_d - \mu N)^n}{n+1} \left( \frac{W/2}{H} \right)^{n+1} + \frac{2}{n+2} \left( \frac{n-2}{n-1} \mu N (\tau_d - \mu N) \right)^{n/2} \left( \frac{y_u}{H} \right)^{\frac{n+2}{2}} + \frac{\mu N^n}{n+1} \right]. \quad (43)$$

152 We see that the first term, which dominates when  $\mu N \ll \tau_d$ , is the SSA expression, while the final term,  
 153 which remains when  $\tau_d = \mu N$ , is the SIA expression. In effect, we have introduced a new term to represent  
 154 the intermediate regime, in which basal drag is significant enough to affect the viscosity, while basal sliding  
 155 remains high enough to affect the surface velocity.

We also consider a further simplification to the model by approximating  $y_u$  as  $W/2$ ,

$$u_{mid}^+ = 2AH \left[ \frac{(\tau_d - \mu N)^n}{n+1} \frac{W/2^{n+1}}{H} + \frac{2}{n+2} \left( \frac{n-2}{n-1} \mu N (\tau_d - \mu N) \right)^{n/2} \left( \frac{W/2}{H} \right)^{\frac{n+2}{2}} + \frac{\mu N^n}{n+1} \right], \quad (44)$$

156 This will systematically overestimate the surface velocity, but in wide channels, this can still provide an  
 157 improved match to the numerical results compared to neglecting the basal shear-thinning entirely (figure  
 158 5). This closed-form expression could readily be inserted into models of ice stream dynamics.

159 Figure 5 shows the difference between the numerically calculated values of  $u_{mid}$  and the three approx-  
 160 imations: SIA plus SSA, (44), and (43). SIA plus SSA significantly underestimates the centreline velocity  
 161 for wide streams with intermediate sliding rates - clearly showing that SSA is valid when  $\mu N/\tau_d \ll 1$ , while  
 162 SIA is valid when  $\mu N/\tau_d \gg H/(W/2)$ , missing the intermediate regime if  $W/2 \gg H$ , where the errors can  
 163 be upwards of 40%. As expected, (44) is an overestimate but increasingly close to the numerical results  
 164 as  $W/2H$  increases. (43) provides the closest match to the numerical results, remaining within 10% of the  
 165 calculated values and only significantly deviating where  $W/2H < 5$  and the shallow approximations break  
 166 down.

## 167 Total flux

168 While surface velocity is most easily measurable, the evolution of ice stream thickness depends on the total  
 169 flux through the stream. We now calculate the ice flux through the stream, again considering the two  
 170 regimes depending on the size of  $\mu N$  compared to  $\tau_d$ .

When  $\mu N$  is small, vertical deformation is negligible, and so the total flux  $Q$  is found by integrating  $u_s H$  across the width of the stream, with  $u_s$  given by (39). Thus we recover the SSA result,

$$Q = 4AH^2 \int_0^{W/2} \frac{(\tau_d - \mu N)^n}{n+1} \left[ \left( \frac{W/2}{H} \right)^{n+1} - \left( \frac{y}{H} \right)^{n+1} \right] dy = 4AH^3 \frac{(\tau_d - \mu N)^n}{n+2} \left( \frac{W/2}{H} \right)^{n+2}. \quad (45)$$

However, if the bed is strong, we divide the flux between the region over the yielded bed, and the region over the unyielded margins. Over the central, yielded region, we have contributions to the flux from both



the basal sliding (37), and the internal deformation (22), such that

$$Q_{inner} = 4AH^2 \int_0^{y_u} \frac{\mu N^n}{n+2} + \frac{2}{n+2} \left( \frac{n-1}{n-2} \mu N (\tau_d - \mu N) \right)^{n/2} \left[ \left( \frac{y_u}{H} \right)^{\frac{n+2}{2}} - \left( \frac{y}{H} \right)^{\frac{n+2}{2}} \right] dy \quad (46)$$

$$= 4AH^3 \left[ \frac{\mu N^n}{n+2} \frac{y_u}{H} + \frac{2}{n+4} \left( \frac{n-1}{n-2} \mu N (\tau_d - \mu N) \right)^{n/2} \left( \frac{y_u}{H} \right)^{\frac{n+4}{2}} \right]. \quad (47)$$

In the margins, we have  $u_b = 0$  and large vertical shear stress. While lateral shear will start to dominate in a region of order  $H$  close to the sidewalls, until then the SIA holds and the velocity is approximately  $y$ -independent, with

$$u = \frac{2AH\tau_b^n}{n+1} \left( \frac{z}{H} \right)^{n+1}. \quad (48)$$

Thus the flux in this outer region is approximately given by

$$Q_{outer} = \frac{4AH^2\tau_b^n}{n+2} \left( \frac{W}{2} - \alpha H - y_u \right), \quad (49)$$

171 where the  $-\alpha H$  represents the reduced flux due to matching onto the no-slip sidewalls. On dimensional  
 172 grounds, we anticipate that the sidewall correction should tend to a constant multiple of  $H$  as  $W/2$   
 173 increases. Numerically it appears that  $\alpha \approx 1.4$  (figure 6). While in the asymptotic limit of  $W/2 \gg H$ , this  
 174 correction is negligible, for moderately wide channels the inclusion of this term provides a simple increase  
 175 in the accuracy of our expression (figure 7). Further analytic progress in this regime is beyond the scope  
 176 of this paper, and further numerical calculations of the non-sliding regime (taking instead a shape-factor  
 177 based approach to the effect of the sidewalls) are found in Nye (1965). For wide channels, this is a small  
 178 correction, and we are primarily interested in the more rapidly sliding regime.

The total flux through the ice stream in the high basal drag regime therefore is approximately given by

$$Q = 4AH^3 \left[ \frac{\mu N^n}{n+2} \frac{W/2 - \alpha H}{H} + \frac{2}{n+4} \left( \frac{n-1}{n-2} \mu N (\tau_d - \mu N) \right)^{n/2} \left( \frac{y_u}{H} \right)^{\frac{n+4}{2}} \right]. \quad (50)$$

Again we suggest that summing the fluxes derived from each limit gives a single expression that transitions accurately between regimes, so

$$Q = 4AH^3 \left[ \frac{\mu N^n}{n+2} \frac{W/2 - \alpha H}{H} + \frac{2}{n+4} \left( \frac{n-1}{n-2} \mu N (\tau_d - \mu N) \right)^{n/2} \left( \frac{y_u}{H} \right)^{\frac{n+4}{2}} + \frac{(\tau_d - \mu N)^n}{n+2} \left( \frac{W/2}{H} \right)^{n+2} \right]. \quad (51)$$

179 As shown in figure 7, this expression is within 10% of the numerically calculated results, far better than

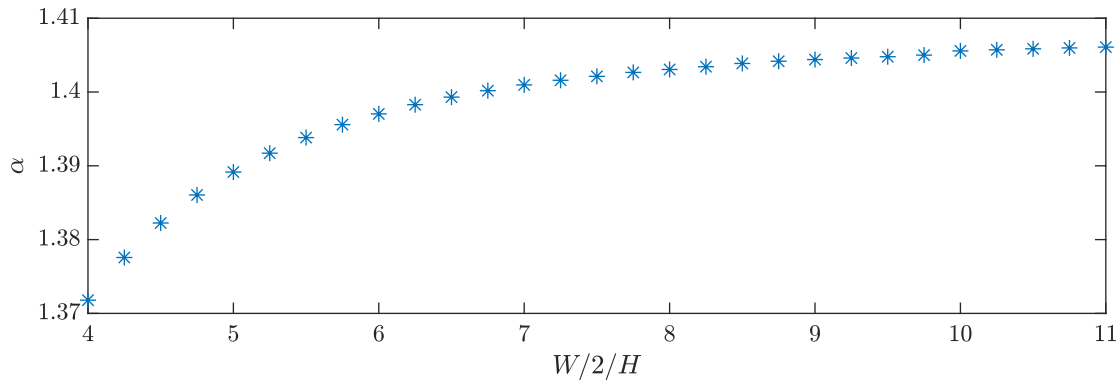


**Fig. 6.** With a no-slip base, the effect of the sidewalls on the flux as summarised by the value of  $\alpha$  in equation (49) tends towards a constant value as  $W/H$  increases.

180 just summing the SSA and SIA values.

As before, a simpler version using  $y_u \approx W/2$  is given by

$$Q_+ = 4AH^3 \left[ \frac{\mu N^n}{n+2} \frac{W/2 - \alpha H}{H} + \frac{2}{n+4} \left( \frac{n-1}{n-2} \mu N (\tau_d - \mu N) \right)^{n/2} \left( \frac{W/2}{H} \right)^{\frac{n+4}{2}} + \frac{(\tau_d - \mu N)^n}{n+2} \left( \frac{W/2}{H} \right)^{n+2} \right], \quad (52)$$

181 and can also provide a good approximation to the numerical results, particularly for wide streams (figure  
 182 7b). However, it is always an overestimate. By contrast, neglecting basal shear-thinning by setting  $y_u = 0$   
 183 and simply summing the SSA and SIA expressions is an underestimate that gets worse for wider streams  
 184 (figure 7a).

## 185 DISCUSSION

186 We have seen that for ice flowing in a stream over a plastic bed, there are three regimes of behaviour for  
 187 the ice flow depending on the yield strength of the bed as compared to the driving stress. If the bed exerts  
 188 very little resistance on the ice, the flow is primarily uniform with depth and resisted by lateral shear from  
 189 the sidewalls (the SSA regime). If the bed strength is high and the ice cannot slide, vertical shear alone  
 190 sets the flow field throughout the majority of the ice stream (the SIA regime). Between these limits is  
 191 a regime where sliding is rapid and lateral stresses are still the primary control on ice speed, but basal  
 192 drag causes shear of significant enough magnitude to soften the ice, thereby altering the response of the  
 193 ice stream away from the margins. We can summarise the effect of this softening through a new term in  
 194 the expressions for surface velocity (43) and flux (51).

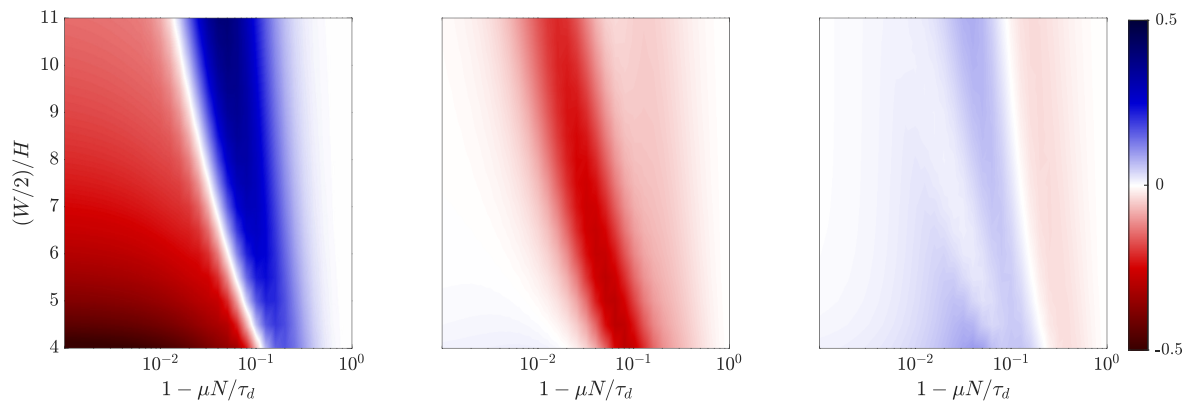


**Fig. 7.** Fractional error in expressions for  $Q$  as compared to the numerically calculated values, for a range of aspect ratios and basal strengths, with  $n = 3$ . a) Sum of SIA and SSA, equation (8) - note this does not include the sidewall modification to the SIA flux, b) including basal shear softening, but with  $y_u$  set to  $W/2$  (52), and c) the full expression (51). Both b) and c) represent improvements over a), with c) the closest match to the numerical results. To guide the eye, the fractional error in b) ranges from -0.29 (at the smallest values of  $W/H$ ) to 0.017 and in c) from -0.036 to 0.098

## 195 Ice-stream geometry and ice rheology

196 We have focused on a rectangular channel geometry which permits several simplifications in our approach.  
 197 Firstly, we take the depth of the ice to be uniform, which considerably simplifies the integration of the  
 198 shear profile across the width of the channel. While a cross-stream variation in ice depth would not alter  
 199 the approach significantly, it would result in more involved analytical calculations. It would also be more  
 200 complex to apply the traction condition on a sloping boundary, although if this slope is small then to  
 201 leading order this correction will be linear in the slope angle. Secondly, in our model setup there is a  
 202 clear separation between the bed of the stream and the sidewalls, allowing us to cleanly impose different  
 203 boundary conditions on each surface. While subglacial sediments may be concentrated in the deepest parts  
 204 of the glacier bed, with sidewalls sloping away from the bed (e.g. Truffer and others, 2001), many ice  
 205 streams in Antarctica are not confined by topography but found between regions of slower-flowing ice. In  
 206 fact, one might consider these streams, generated by variations in bed strength, as an extreme example  
 207 of a very wide channel in which only a narrow central section of the bed has yielded, and any actual  
 208 sidewalls play negligible role. Interestingly, this suggests that basal-stress controlled streams could show  
 209 a different dependence of speed on their width and bed strength than topographically-controlled streams.  
 210 The flow of ice over a flat bed with variable bed strength is considered in Schoof (2004) - the self-consistent

211 determination of the yielded regions of the bed are key to solving for the stress field in this geometry.

212 We have taken our flow to be uniform in the along-flow direction, which reduces the dimensionality of  
213 the problem and removes any extensional stresses. This simplifies the expression for the effective viscosity,  
214 as we have assumed either basal shear or lateral shear must dominate in any region of the stream. In fact,  
215 at the centre of an ice-stream, extensional stresses will dominate if along-flow velocity variations over a  
216 distance comparable to the stream width are large relative to maximum flow speeds. Including extensional  
217 stresses also introduces longitudinal terms in the force balance. However, we suggest that a comparison of  
218 extensional to lateral stresses in a freely sliding regime is better left to two-dimensional membrane models.  
219 Once the dominant horizontal stress relevant to the geometry is identified, one can introduce basal drag  
220 either using this work, or the analysis of Schoof and Hindmarsh (2010), who looked at basal drag as a  
221 perturbation to extensional flow.

222 In taking a simple power-law rheology for the ice, we have ignored the complex dependence of ice  
223 viscosity on a host of factors, but most pertinently temperature, water content, damage, and fabric (grain  
224 size and orientation). All of these factors are particularly likely to differ between the bulk of the ice stream  
225 and the regions of highest shear, namely in the shear margins and close to the bed (Harrison and others,  
226 1998; Minchew and others, 2018). By considering these as additional mechanisms by which the ice viscosity  
227 depends on shear rate, one could attempt to parametrise their effects by using an altered power  $n$  in the  
228 ice rheology. As such, we have left all the expressions in our results as holding for general  $n$ . However, the  
229 flow of ice advects heat, damage, and water downstream, so the dependence of viscosity on shear rate can  
230 be non-local in a way which cannot be fully captured by this steady, uniform model.

231 We note that all these assumptions in our model setup are common when working with simplified  
232 models of ice stream flow. However, it is worth considering, and exploring with more detailed numerical  
233 models, whether including basal shear-softening and more accurately capturing flow in this geometry is  
234 significant compared to the error introduced by simplifying the ice stream geometry and rheology in the  
235 first place.

### 236 **Approximations in the analysis**

237 Our mathematical analysis is not of the full-Stokes equations (1) directly, but of an approximation using  
238 a linear shapefactor for the vertical shear stress. This approximation can be motivated by the separation  
239 of scales between the horizontal and vertical velocity gradients for wide streams, and the numerical stress

240 fields (figure 2) reassure that the approximation is reasonable. Further, the L1L2 model on which it is  
241 based is well-tested compared to full-Stokes simulations. However, this approximation breaks down for  
242 narrow streams over strong beds, as can be seen in figure 5.

243 Indeed, a question remains as to what happens close to the sidewalls when the bed is not sliding. As  
244 discussed in the results, close to the sidewalls the surface velocity and basal stress go to zero across a region  
245 of width  $\sim H$ , which leads to errors in the estimated flux through the ice stream. Numerical analysis of  
246 this problem dates back to Nye (1965); Kozicki and others (1966), but to our knowledge no analytic results  
247 exist for the flow of shear-thinning fluids near a corner. The problem is inherently two-dimensional, with  
248 significant vertical gradients in horizontal stress that the L1L2 approach is not designed to handle. Further  
249 study of these dynamics are certainly interesting from a fluid-dynamical perspective, but beyond the scope  
250 of the present paper.

251 We have calculated the centreline surface velocity in a manner that avoids considering the velocity field  
252 above the unyielded region, but our estimate of  $y_u$  becomes less accurate as the region widens. Since our  
253 estimate of  $y_u$  does tend to 0 as  $\mu N \rightarrow \tau_d$ , we have the correct leading order expressions for  $u_{mid}$  and  $Q$  in  
254 this regime. However, the estimate of sliding speed depends directly on  $y_u$  and could therefore be improved  
255 by more detailed calculation of the dynamics above the unyielded bed (c.f. Haseloff and others, 2019).

### 256 Cross-stream surface velocity profiles

257 Understanding the full flow-field close to the sidewalls would allow us to predict not just the centreline  
258 speed and surface velocity over the unyielded sections of the bed, but also the entire surface velocity profile  
259 into the margins. In our numerical results, we see appreciable changes in surface velocity profile as the bed  
260 strength increases (figure 8), with the width of the shear margins initially widening then narrowing to less  
261 than those of the SSA profile.

Initially, as the basal drag increases, basal shear-softening reduces the effective viscosity in the centre  
of the stream, leading to larger shear rates there, and more rounded velocity profiles ( $u_{mid} - u_s \sim y^{(n+2)/2}$ )  
compared to the freely-sliding case ( $u_{mid} - u_s \sim y^{n+1}$ ). As bed strength increases further, the unyielded  
regions of the bed encroach towards the centre of the stream. The shear margins are concentrated over  
the non sliding regions (c.f. Truffer and others, 2001), and numerically we see that the shape of these  
margins closely resembles surface velocity profile for a completely static bed. We therefore suggest that an  
approximate expression for the surface velocity profile over the entire stream can be found, similarly to the

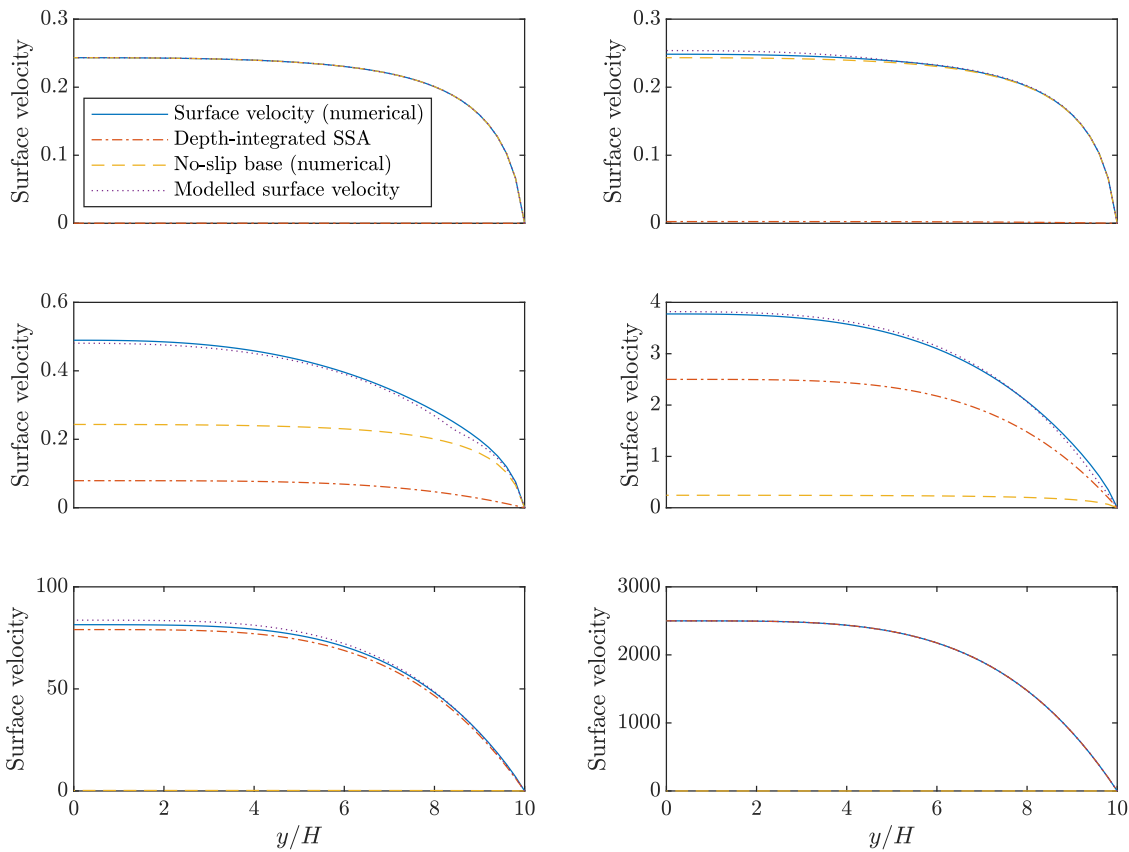


**Fig. 8.** Numerically calculated profiles of surface velocity for for increasing values of  $1 - \mu N/\tau_d = 10^{-2.5}, 10^{-2}, 10^{-1.5}, 10^{-1}, 10^{-0.5}, 1$ , compared to the SSA profile (39), the numerically calculated surface velocity with  $u_b = 0$ , and the model we propose in (53), taking into account basal shear softening. The velocities are scaled so that  $2A\tau_d^3 H^4 = 1$ .

method by which the centre-line velocity was found in (43), by summing the SSA solution, the numerically calculated profile for non-sliding bed, and a term representing effect of basal shear softening where  $y < y_u$ ,

$$u_s(y) \approx u_s(y, u_b = 0) + 2AH \frac{(\tau_d - \mu N)^n}{n+1} \left[ \left( \frac{W/2}{H} \right)^{n+1} - \left( \frac{y}{H} \right)^{n+1} \right] + \frac{4AH}{n+2} \left( \frac{n-2}{n-1} \mu N (\tau_d - \mu N) \right)^{n/2} \max \left[ \left( \frac{y_u}{H} \right)^{\frac{n+2}{2}} - \left( \frac{y}{H} \right)^{\frac{n+2}{2}}, 0 \right] \quad (53)$$

262 The surface velocity profile reveals more information about the bed and ice rheology than the centre-line  
 263 speed alone. Simple expressions for surface velocity have been used to estimate ice depth or basal properties  
 264 (e.g. Li and others, 2012) before recourse to full-Stokes modelling, and our improved estimate of surface  
 265 velocity could feed into such work. However, with uncertainties in ice rheology, bed geometry, and basal  
 266 conditions, it is not possible to simultaneously invert for all unknowns from only a single value, namely  
 267 maximum surface velocity. In large-scale inversions, the spatial heterogeneity of surface velocity is used as  
 268 a constraint. In a similar manner, the width of the shear margins and the degree of uniformity across the  
 269 centre of the stream could provide sufficient constraints to simultaneously constrain ice rheology and basal  
 270 strength. This could be used to e.g. extend the work of Millstein and others (2022), approximating ice  
 271 rheology, to grounded ice streams, or re-examine Minchew and others (2018) beyond the use of the SSA  
 272 approximation.

### 273 **Applicability to other sliding laws**

274 While previous work employing simple expressions for sliding speed and flux through ice streams has mainly  
 275 centred on flow over a bed of uniform strength, larger scale ice sheet models more frequently use regularised  
 276 sliding laws. Here we consider to what extent our results for a constant-strength bed are applicable to  
 277 sliding laws of the form  $u_b = f(\tau_b)$ .

If we view our results as a calculation for the basal sliding speed  $u_b(\tau_b)$ , flux  $Q(\tau_b)$ , and surface velocity  $u_s(\tau_b)$  for a given basal traction, we can look for self-consistent solutions to

$$f(\tau_b) = u_b(\tau_b), \quad (54)$$

278 effectively approximating the basal traction as its value in the centre of the bed. This allows us to predict  
 279 the surface velocity and flux as functions of the sliding law and driving stress, which we can again compare

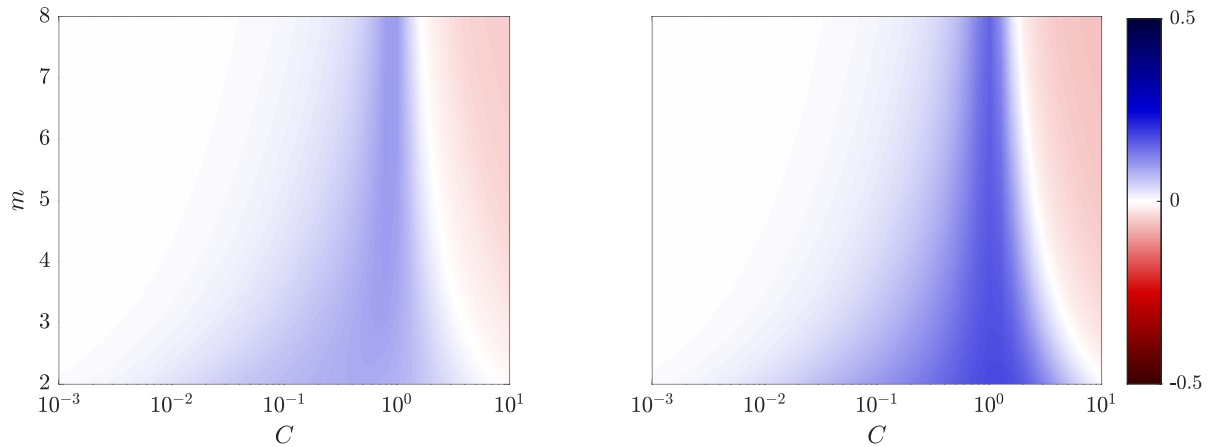


**Fig. 9.** Fractional error in estimated (left) centreline surface velocity  $u_{mid}$  and (right) total flux  $Q$  using (54), compared to numerically calculated results with a sliding law of the form (56), for  $n = 3$  and  $(W/2)/H = 8$ .

280 to numerically calculated values.

Based on our expression for maximum sliding speed,

$$u_b(\tau_b) = 2AH \left[ \frac{(\tau_d - \tau_b)^n W/2^{n+1}}{n+1} \frac{1}{H} + \frac{2}{n+2} \left( \frac{n-2}{n-1} \tau_b (\tau_d - \tau_b) \right)^{n/2} \left( \frac{W/2}{H} - \frac{\tau_b H}{2(\tau_d - \tau_b)(W/2)} \right)^{\frac{n+2}{2}} \right] \quad (55)$$

281 we cannot directly solve this implicit equation for  $u_b$  or  $\tau_b$  in general, but it remains a computationally  
282 cheap problem compared to numerical solution of the Stokes equations.

Considering a power-law sliding law of the form

$$\tau_b = C u_b^{1/m}, \quad (56)$$

we see generally reasonable agreement between the numerical and self-consistently calculated values of  $Q$  and  $u_{mid}$  (figure 9). However, the clearest difference between the numerical velocity fields for the plastic bed and power-law sliding is in the surface velocity profiles for very strong beds (large  $C$ ). This can be attributed to the difference in the shape of the basal velocity profiles as  $u_b \rightarrow 0$ . Over a plastic bed, the margins stop yielding while the centre of the bed continues to slide, the ice above which is resisted primarily by lateral shear - this leads to fairly rounded surface velocity profiles. Over a power-law bed, once  $\tau_b \sim \tau_d$ , one can rearrange (56) to find a constant sliding speed  $u_b = (\tau_d/C)^m$  over the majority of the bed, and without lateral variations in sliding speed, the vertical shear stress dominates the force balance, leading to



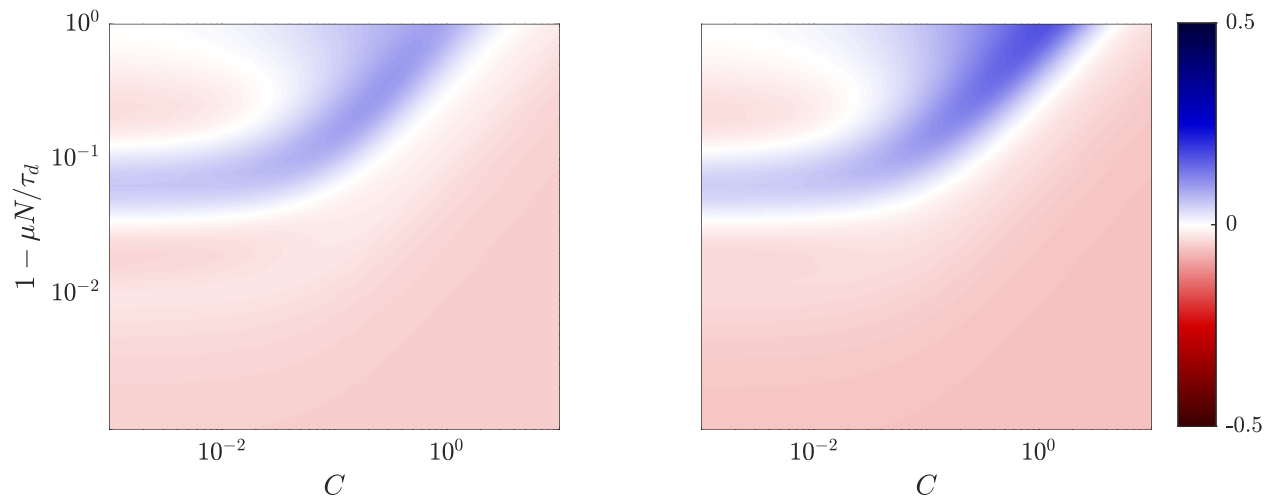


**Fig. 10.** Fractional error in estimated (left) centreline surface velocity  $u_{mid}$  and (right) total flux  $Q$  using (54), compared to numerically calculated results with a sliding law of the form (58) with  $m = 3$ , for  $n = 3$  and  $(W/2)/H = 8$ .

a correspondingly uniform surface velocity

$$u_s \approx \frac{\tau_d^m}{C} + \frac{2A\tau_d^n H}{n+1}, \quad (57)$$

with shear margins of order  $H$  close to the sidewalls.

We can also look at the impact of mixed sliding laws of the form

$$\tau_b = \mu N + C u_b^{1/m}, \quad (58)$$

which would correspond to a visco-plastic material at the bed (Iverson, 2010; Warburton and others, 2023).

As might be expected, this gives qualitatively similar results to the plastic bed when  $C$  is small, and similar results to the power-law bed when  $C$  is large. In both regimes the self-consistent method for calculating  $\tau_b$  leads to reasonable agreement with numerically calculated values of  $Q$  and  $u_{mid}$  (figure 10).

The comparisons suggest that our simple expressions for flux and velocity can produce useful results for more general sliding laws, by seeking self-consistent values of basal drag and basal sliding. It again suggests that surface velocity profiles are a key indicator of basal boundary conditions.

Alternatively, we can view the expression for sliding speed as a function of basal shear stress as a mixed boundary condition that an ice stream exerts on its bed. It could be used as a more ice-stream-representative boundary condition in studies of till dynamics, beyond forcing with a constant shear stress

294 or speed.

## 295 CONCLUSIONS

296 By considering the impact of basal drag on depth-integrated viscosity, we have produced improved expres-  
297 sions for the velocity field in an ice-stream flowing over a bed of constant yield-strength which capture the  
298 transition from the sidewall-resisted regime into the basal shear dominated regime. These more accurate  
299 expressions for the basal sliding speed (55), surface velocity (43), and total flux (51) through the stream  
300 are simple enough to include in wider models of the interaction of ice streams with their environment, and  
301 could also be used to rapidly invert for bed properties given surface observations. While we have focused on  
302 a simple geometry and simple ice rheology, these results still provide an improved estimate of ice behaviour  
303 under these oft-assumed conditions.

## 304 ACKNOWLEDGEMENTS

305 KLPW is supported by a postdoctoral fellowship from the Dartmouth Society of Fellows. Some of this  
306 work formed part of KLPW's doctorate, supported by the Natural Environment Research Council (grant  
307 no. NE/L002507/1), on which Grae Worster and Andrew Hogg provided helpful comments. The authors  
308 also thank Logan Mann and Brent Minchew for useful conversations.

## 309 REFERENCES

- 310 Adhikari S and Marshall S (2012) Parameterization of lateral drag in flowline models of glacier dynamics. *J. Glaciol.*,  
311 **58**(212), 1119–1132 (doi: 10.3189/2012JoG12J018)
- 312 Benn DI, Hulton NR and Mottram RH (2007) 'calving laws', 'sliding laws' and the stability of tidewater glaciers.  
313 *Annals of Glaciology*, **46**, 123–130 (doi: 10.3189/172756407782871161)
- 314 Blatter H (1995) Velocity and stress fields in grounded glaciers: a simple algorithm for including deviatoric stress  
315 gradients. *J. Glaciol.*, **41**(138), 333–344 (doi: 10.3189/S002214300001621X)
- 316 Cuffey KM and Paterson WSB (2010) *The physics of glaciers*. Academic Press
- 317 Fowler A (2011) *Mathematical Geoscience*. Interdisciplinary Applied Mathematics, Springer Science & Business  
318 Media, ISBN 978-0-85729-699-3 (doi: 10.1007/978-0-85729-721-1)

- 319 Glen JW (1955) The creep of polycrystalline ice. *Proc. R Soc. London, Ser. A*, **228**(1175), 519–538 (doi:  
320 10.1098/rspa.1955.0066)
- 321 Goldberg DN and Sergienko OV (2011) Data assimilation using a hybrid ice flow model. *Cryosphere*, **5**, 315–327 (doi:  
322 10.5194/tc-5-315-2011)
- 323 Goldsby DL and Kohlstedt DL (2001) Superplastic deformation of ice: Experimental observations. *J. Geophys. Res.:  
324 Solid Earth*, **106**(B6), 11017–11030 (doi: 10.1029/2000JB900336)
- 325 Harrison WD, Echelmeyer KA and Larsen CF (1998) Measurement of temperature in a margin of Ice  
326 Stream B, Antarctica: implications for margin migration and lateral drag. *J. Glac.*, **44**(148), 615–624 (doi:  
327 10.3189/S0022143000002112)
- 328 Haseloff M, Hewitt IJ and Katz RF (2019) Englacial pore water localizes shear in temperate ice stream margins. *J.  
329 Geophys. Res.: Earth Surface*, **124**(11), 2521–2541 (doi: <https://doi.org/10.1029/2019JF005399>)
- 330 Hindmarsh RCA (2004) A numerical comparison of approximations to the Stokes equations used in ice sheet and  
331 glacier modeling. *J. Geophys. Res.: Earth Surface*, **109**(F1) (doi: <https://doi.org/10.1029/2003JF000065>)
- 332 Hunter P, Meyer C, Minchew B, Haseloff M and Rempel A (2021) Thermal controls on ice stream shear margins. *J.  
333 Glac.*, **67**(263), 435–449 (doi: 10.1017/jog.2020.118)
- 334 Iverson NR (2010) Shear resistance and continuity of subglacial till: hydrology rules. *J. Glaciol.*, **56**(200), 1104–1114  
335 (doi: 10.3189/002214311796406220)
- 336 Joughin I, Smith BE and Schoof CG (2019) Regularized Coulomb Friction Laws for Ice Sheet Slid-  
337 ing: Application to Pine Island Glacier, Antarctica. *Geophys. Res. Lett.*, **46**(9), 4764–4771 (doi:  
338 <https://doi.org/10.1029/2019GL082526>)
- 339 Kamb B (2001) *Basal Zone of the West Antarctic Ice Streams and its Role in Lubrication of Their Rapid Motion*,  
340 157–199. American Geophysical Union (AGU), ISBN 9781118668320 (doi: <https://doi.org/10.1029/AR077p0157>)
- 341 Kamb B and Echelmeyer KA (1986) Stress-gradient coupling in glacier flow: I. longitudinal averaging of the influence  
342 of ice thickness and surface slope. *J. Glac.*, **32**(111), 267–284 (doi: 10.3189/S0022143000015604)
- 343 Kozicki W, Chou C and Tiu C (1966) Non-Newtonian flow in ducts of arbitrary cross-sectional shape. *Chem. Eng.  
344 Sci.*, **21**(8), 665–679, ISSN 0009-2509 (doi: [https://doi.org/10.1016/0009-2509\(66\)80016-7](https://doi.org/10.1016/0009-2509(66)80016-7))
- 345 Li H, Ng F, Li Z, Qin D and Cheng G (2012) An extended “perfect-plasticity” method for estimating  
346 ice thickness along the flow line of mountain glaciers. *J. Geophys. Res.: Earth Surface*, **117**(F1) (doi:  
347 <https://doi.org/10.1029/2011JF002104>)

- 348 MacAyeal DR (1989) Large-scale ice flow over a viscous basal sediment: Theory and application to ice stream b,  
349 antarctica. *J. of Geophys. Res.: Solid Earth*, **94**(B4), 4071–4087 (doi: <https://doi.org/10.1029/JB094iB04p04071>)
- 350 Mann LE, Robel AA and Meyer CR (2021) Synchronization of Heinrich and Dansgaard-Oeschger Events Through Ice-  
351 Ocean Interactions. *Paleocean. Paleoclim.*, **36**(11), e2021PA004334 (doi: <https://doi.org/10.1029/2021PA004334>),  
352 e2021PA004334 2021PA004334
- 353 Meyer CR and Minchew BM (2018) Temperate ice in the shear margins of the Antarctic Ice Sheet: Con-  
354 trolling processes and preliminary locations. *Earth Planet. Sci. Lett.*, **498**, 17–26, ISSN 0012-821X (doi:  
355 <https://doi.org/10.1016/j.epsl.2018.06.028>)
- 356 Millstein JD, Minchew BM and Pegler SS (2022) Ice viscosity is more sensitive to stress than commonly assumed.  
357 *Commun. Earth Environ.*, **3**(1), 57, ISSN 2662-4435 (doi: [10.1038/s43247-022-00385-x](https://doi.org/10.1038/s43247-022-00385-x))
- 358 Minchew B, Simons M, Bjornsson H, Palsson F, Morlighem M, Seroussi H, Larour E and Hensley S (2016) Plastic  
359 bed beneath Hofsjökull Ice Cap, central Iceland, and the sensitivity of ice flow to surface meltwater flux. *J. Glac.*,  
360 **62**(231), 147–158 (doi: [10.1017/jog.2016.26](https://doi.org/10.1017/jog.2016.26))
- 361 Minchew BM and Meyer CR (2020) Dilation of subglacial sediment governs incipient surge motion in glaciers with  
362 deformable beds. *Proc. R. Soc. A*, **476**(2238), 20200033 (doi: [10.1098/rspa.2020.0033](https://doi.org/10.1098/rspa.2020.0033))
- 363 Minchew BM, Simons M, Riel B and Milillo P (2017) Tidally induced variations in vertical and horizontal motion on  
364 Rutford Ice Stream, West Antarctica, inferred from remotely sensed observations. *J. Geophys. Res. Earth Surface*,  
365 **122**(1), 167–190 (doi: [10.1002/2016JF003971](https://doi.org/10.1002/2016JF003971))
- 366 Minchew BM, Meyer CR, Robel AA, Gudmundsson GH and Simons M (2018) Processes controlling the downstream  
367 evolution of ice rheology in glacier shear margins: case study on Rutford Ice Stream, West Antarctica. *J. Glaciol.*,  
368 **64**(246), 583–594 (doi: [10.1017/jog.2018.47](https://doi.org/10.1017/jog.2018.47))
- 369 Morland LW (1987) Unconfined ice-shelf flow. In CJ Van der Veen and J Oerlemans (eds.), *Dynamics of the West*  
370 *Antarctic Ice Sheet*, 99–116, Springer Netherlands, Dordrecht, ISBN 978-94-009-3745-1
- 371 Nye JF (1965) The flow of a glacier in a channel of rectangular, elliptic or parabolic cross-section. *J. Glaciol.*, **5**(41),  
372 661–690 (doi: [10.3189/S0022143000018670](https://doi.org/10.3189/S0022143000018670))
- 373 Pattyn F (2003) A new three-dimensional higher-order thermomechanical ice sheet model: Basic sensitivity,  
374 ice stream development, and ice flow across subglacial lakes. *J. Geophys. Res.: Solid Earth*, **108**(B8) (doi:  
375 <https://doi.org/10.1029/2002JB002329>)
- 376 Raymond C (1996) Shear margins in glaciers and ice sheets. *J. Glac.*, **42**(140), 90–102 (doi:  
377 [10.3189/S0022143000030550](https://doi.org/10.3189/S0022143000030550))

- 378 Rosier SHR, Gudmundsson GH and Green JAM (2015) Temporal variations in the flow of a large Antarctic ice  
379 stream controlled by tidally induced changes in the subglacial water system. *The Cryosphere*, **9**(4), 1649–1661  
380 (doi: 10.5194/tc-9-1649-2015)
- 381 Schoof C (2004) On the mechanics of ice-stream shear margins. *J. Glac.*, **50**(169), 208–218 (doi:  
382 10.3189/172756504781830024)
- 383 Schoof C (2006) Variational methods for glacier flow over plastic till. *J. Fluid Mech.*, **555**, 299–320 (doi:  
384 10.1017/S0022112006009104)
- 385 Schoof C and Hindmarsh RCA (2010) Thin-film flows with wall slip: An asymptotic analysis of higher order glacier  
386 flow models. *Q. J. Mech. Appl. Math.*, **63**(1), 73–114, ISSN 0033-5614 (doi: 10.1093/qjmam/hbp025)
- 387 Truffer M, Echelmeyer KA and Harrison WD (2001) Implications of till deformation on glacier dynamics. *J. Glac.*,  
388 **47**(156), 123–134 (doi: 10.3189/172756501781832449)
- 389 Warburton KLP, Hewitt DR and Neufeld JA (2023) Shear dilation of subglacial till results in time-dependent sliding  
390 laws. *Proc. R Soc. A*, **479**(2269), 20220536 (doi: 10.1098/rspa.2022.0536)
- 391 Weertman J (1957) On the sliding of glaciers. *J. Glaciol.*, **3**(21), 33–38 (doi: 10.3189/S0022143000024709)